INTERNATIONAL JOURNAL FOR NUMERICAL METHODS IN FLUIDS
Int. J. Numer. Meth. Fluids 2008; **57**:1137–1152
Published online 14 April 2008 in Wiley InterScience (www.interscience.wiley.com). DOI: 10.1002/fld.1781

Stabilized edge-based finite element computation of gravity currents in lock-exchange configurations

Renato N. Elias[1], Paulo L. B. Paraizo[2] and Alvaro L. G. A. Coutinho[1,*,†]

[1]*Center for Parallel Computations and Department of Civil Engineering, Federal University of Rio de Janeiro, P.O. Box 68506, RJ 21945-970, Rio de Janeiro, Brazil*
[2]*Petrobras Research Center, Production Division, Av. Horacio Macedo, 850, Rio de Janeiro, Brazil*

SUMMARY

Modeling of gravity current flows is important in many problems of science and engineering. Gravity currents are primarily horizontal flows driven by a density difference of few per cents. This phenomenon occurs in many scales in nature, such as ocean and marine flows, sea breeze formation, avalanches, turbidite flows, etc. Most of the gravity current simulations employ structured grid or spectral methods. In this work, we simulate gravity-driven flows by a parallel stabilized edge-based finite element code with particular emphasis on the simulation of the lock-exchange problem for planar and cylindrical configurations. Our results are validated against other highly resolved numerical simulations and experiments. Copyright © 2008 John Wiley & Sons, Ltd.

Received 12 September 2007; Revised 7 January 2008; Accepted 7 January 2008

KEY WORDS: gravity currents; stabilized finite elements; edge-based data structures

1. INTRODUCTION

Gravity current occurs when an amount of fluid displaces due to a difference in the density caused by differences in temperature, fine grain particles in suspension, salinity or the mixture between fluids [1]. Severe squalls associated with thunderstorms, where a cloud of cold air suddenly displaces horizontally mixing with hot air close to the seashore, the formation of sea-breeze in coastal areas, displacement of piroclastic clouds discharged by volcanoes, turbidity currents formed by the discharge of sediments arising from rivers into the sea,

*Correspondence to: Alvaro L. G. A. Coutinho, Center for Parallel Computations and Department of Civil Engineering, Federal University of Rio de Janeiro, P.O. Box 68506, RJ 21945-970, Rio de Janeiro, Brazil.
†E-mail: alvaro@nacad.ufrj.br

Contract/grant sponsor: CNPq; contract/grant number: 301.251/2005-3
Contract/grant sponsor: Petroleum National Agency (ANP/Brazil)

snow avalanches and leakage of heavy gases, are practical examples of gravity currents of scientific relevance [1]. Particularly, turbidity currents are a very efficient transport mechanism of an enormous amount of sand. According to Lucchesi [2], this is the main formation mechanism of rocks called turbidites. These rocks host the majority of offshore oil reserves in Brazil.

There exists a large concern in the scientific community for experimental studies to help in understanding this kind of flows. Most of these studies are focused on idealized hypothesis, where the main aspects related to gravity currents are treated in a simplified or isolated manner. These works frequently employ simple geometries with flows restricted to channels where the main features of the flow can be easily understood and studied. For a review regarding experimental and theoretical works about gravity currents, we suggest [1]. Experimental studies such as those by Neufeld [3], Shin *et al.* [4] and Marino *et al.* [5] are important to understand the dynamics of gravity currents and the global features of the flow, such as the lobe and cleft mechanisms. However, there has been an increasing use of numerical methods to model gravity currents, mainly due to the growth in the computational resources and the development of efficient numerical software in the past decades. Most of these numerical studies have focused on structured grids and spectral methods employing a direct numerical simulation (DNS) approach where even the fine scales of the flow are represented [6–11]. Recently, a comprehensive study on the dynamics of the front velocity during the different phases of spreading, namely, acceleration, slumping, inertial and viscous phases, has been carried out by Cantero *et al.* [12]. It involved highly resolved three-dimensional and two-dimensional simulations in planar and cylindrical configurations. They verified that two-dimensional simulations underpredict the front location and velocity during the spreading phases, but the structure and dynamics of the three-dimensional currents were in good agreement with previously reported numerical and experimental observations.

Such works are important since they are also able to supply detailed information about lobes and cleft formation, characteristic structures of gravity currents. On the other hand, the DNS requires a large computational cost, even for modern computers and solvers. Incorporating a turbulence model to reduce the need to account for all the small scales of the flow can decrease computing time significantly. Large eddy simulation (LES) is a technique where the large scales of the flow are fully resolved with a model being used to account for the small scales. This is based on filtering the Navier–Stokes equations to separate the large scales from the small (see Sagaut *et al.* [13]). In Ooi [14] and Ooi *et al.* [15], a detailed study of three-dimensional lock-exchange gravity flow is performed using a non-uniform Cartesian mesh finite volume LES code with a dynamic Smagorinsky model as described by Pierce and Moin [16]. These studies demonstrated that 3D LES is able to correctly capture most of the important aspects of lock-exchange gravity-driven flows at high Grashof numbers where DNS simulations are computationally too expensive. For complex geometries of practical interest, however, such as those found in coastal lines, mountains, ocean bathymetry, canyons, etc., DNS or LES on structured grids suffer from severe geometrical constraints. According to Pain *et al.* [17], unstructured grid methods, such as finite elements and finite volumes, handle the complex geometries found in these natural scenarios very easily and form an excellent framework for modeling gravity currents in coarse and fine scales.

A first attempt towards the simulation of gravity currents by stabilized finite elements was performed by Cantero *et al.* [18], employing a flow description based on the Reynolds averaged

DOI: 10.1002/fld

equations and a closure model. Their three-dimensional simulation of a lock-exchange device, where a denser fluid consisting of a salt–water mixture displaces fresh water, showed good agreement with experimental measurements. Nevertheless, several works indicate that numerical viscosities generated by stabilized methods act as Smagorinsky-like eddy viscosities present in LES [19–23]. Indeed, the works of Guasch and Codina [24] and de Sampaio *et al.* [25] provide support, with different arguments, to the idea that no extra physical LES modeling should be added to the equations. For the orthogonal subgrid scale stabilized finite element method, Guasch and Codina [24] proved that the contribution to the energy balance equations of the stabilized terms is proportional to the physical dissipation rate. In [25] it was shown that a particular stabilized finite element method is equivalent to the use of a Galerkin method on the spatially filtered equations, where a particular subgrid model, proportional to the discretization residual, is applied. Another interpretation is provided in [26], which recognizes that introducing some form of dissipation is essentially adapting the physical and mathematical models to accommodate a deficiency in the choice of mesh, that is, incorporating subgrid effects. Therefore, in this work we attempt the computational simulation of turbulent gravity currents by a stabilized edge-based finite element method with no explicit model for subgrid scales other than the one intrinsically induced by the numerical method itself. The finite element method is an edge-based streamline-upwind/Petrov–Galerkin and pressure-stabilizing/Petrov–Galerkin (SUPG/PSPG) formulation. For recent reviews of stabilized finite element methods, we refer to Tezduyar [27] and Tezduyar and Sathe [28].

Edge-based data structures have been introduced in the finite element context to speed up explicit compressible flow simulations (see Lohner [29]). More recently, Ribeiro *et al.* [30] presented an edge-based implementation for stabilized semi-discrete and space–time finite element formulations for shallow water equations, Catabriga and Coutinho [31] for the implicit SUPG solution of the Euler equations, Soto *et al.* [32] for incompressible flow problems with fractional step methods and Kraft *et al.* [33] for a segregated symmetric stabilized solution of incompressible flow with heat transfer and the parallel simulation of viscoplastic and free surface flows [34, 35]. It has been shown by Ribeiro and Coutinho [36] that, for unstructured grids composed by tetrahedra, edge-based data structures decrease the number of floating point operations and indirect addressings in matrix–vector products needed in the Krylov space solvers and diminish the storage area to hold Jacobians compared with element and pointwise data structures, particularly for problems involving many degrees of freedom. The construction of edge operations are completely algebraic [30, 31, 33–35], based on the concept of disassembling element operators, regardless of the particular underlying finite element formulation, thus providing a fast platform for simulation of complex problems such as those found in the present work.

Validations of the present approach are performed for head current position and velocity against DNS and LES simulations previously presented in [7, 8, 10, 12, 14, 37] for planar and cylindrical lock-exchange configurations. For the planar case, we also compare our results with the experiments of Shin *et al.* [4]. These parameters were chosen since they are important to study the ability of the gravity current to transport sediments for long distances and explain how the sedimentation and erosional processes take place [38].

In the remainder of this paper, the governing equations and finite element formulation are presented in Section 2, the solution procedure in Section 3, the test problems in Section 4 and conclusions and final remarks summarized in Section 5.

DOI: 10.1002/fld

2. GOVERNING EQUATIONS

This section presents the governing equations for incompressible fluid flow and advection–diffusion transport of the gravity current as well as the corresponding stabilized edge-based finite element formulations.

2.1. Incompressible flow and gravity current transport

Let us consider the spatial domain given by $\Omega \subset \Re^{n_{\text{dim}}}$, where n_{dim} is the number of spatial dimensions and Γ the boundary of Ω. In this work, we consider the velocity–pressure formulation of the Navier–Stokes equations in dimensionless form to describe the incompressible fluid flow of two immiscible fluids with densities $\tilde{\rho}_0$ and $\tilde{\rho}_1$, following the Boussinesq hypothesis where the density differences are small, typically not larger than 5%. Thus, the dimensionless equations are

$$\frac{\partial \mathbf{u}}{\partial t} + \mathbf{u} \cdot \nabla \mathbf{u} - \rho \mathbf{g} = \nabla \cdot \boldsymbol{\sigma} \quad \text{in } \Omega \times [0, t_{\text{f}}] \tag{1}$$

$$\nabla \cdot \mathbf{u} = \mathbf{0} \quad \text{in } \Omega \times [0, t_{\text{f}}] \tag{2}$$

$$\boldsymbol{\sigma}(\mathbf{u}, p) = p\mathbf{I} + \frac{2}{\sqrt{Gr}} \boldsymbol{\varepsilon}(\mathbf{u}) \tag{3}$$

$$\varepsilon(\mathbf{u}) = \tfrac{1}{2}(\nabla \mathbf{u} + (\nabla \mathbf{u})^{\text{T}}) \tag{4}$$

$$\frac{\partial \rho}{\partial t} + \mathbf{u} \cdot \nabla \rho - \nabla \cdot \left(\left(\frac{1}{Sc\sqrt{Gr}} \right) \nabla \rho \right) = 0 \quad \text{in } \Omega \times [0, t_{\text{f}}] \tag{5}$$

where ρ is the dimensionless density fluctuation, $\rho = (\tilde{\rho} - \tilde{\rho}_0)/(\tilde{\rho}_1 - \tilde{\rho}_0)$, $\mathbf{u}$, p and t the dimensionless velocity, pressure and time, respectively. Here, $\mathbf{g}$ is a unit vector pointing in the gravity direction and Gr is the Grashof number; a dimensionless relationship between the buoyancy and viscous forces is given by

$$Gr = \left(\frac{U_0}{\nu h_0} \right)^2 \tag{6}$$

where ν is the kinematic viscosity, h_0 is a characteristic length of the flow, $U_0 = \sqrt{g h_0 (\tilde{\rho}_1 - \tilde{\rho}_0)}/\tilde{\rho}_0$ is the buoyancy velocity, g is the gravity acceleration and Sc is the Schmidt number,

$$Sc = \frac{\nu}{\kappa} \tag{7}$$

where κ is the diffusivity of the quantity responsible for the density difference. Essential and natural boundary conditions for Equation (1) are $\mathbf{u} = \mathbf{g}$ on $\Gamma_{\mathbf{g}}$ and $\mathbf{n} \cdot \boldsymbol{\sigma} = \mathbf{h}$ on $\Gamma_{\mathbf{h}}$, where $\Gamma_{\mathbf{g}}$ and $\Gamma_{\mathbf{h}}$ are complementary subsets of the domain boundary Γ. Functions $\mathbf{g}$ and $\mathbf{h}$ are given and $\mathbf{n}$ is the unit outward normal vector of Γ. A divergence-free velocity field $\mathbf{u}_0(\mathbf{x})$ is the initial condition of Equation (1). For Equation (5) the essential and natural boundary conditions are $\rho = g_\rho$ on Γ_g^ρ and $\mathbf{n} \cdot (1/Sc\sqrt{Gr}) \nabla \rho = h_\rho$ on Γ_h^ρ, where Γ_g^ρ and Γ_h^ρ are complementary subsets of Γ and g_ρ and h_ρ are given functions. The initial condition for Equation (5) is $\rho_0(\mathbf{x})$.

DOI: 10.1002/fld

2.2. Finite element formulation

For the weak form of Equations (1)–(4), we assume the following weight and trial function spaces for the velocity and pressure: $S_{\mathbf{u}}^h$, $V_{\mathbf{u}}^h$, S_p^h and $V_p^h = S_p^h$. The finite element method corresponding to the SUPG/PSPG formulation for the incompressible flow can be expressed as follows: find $\mathbf{u}^h \in S_{\mathbf{u}}^h$ and $p^h \in S_p^h$ such that $\forall \mathbf{w}^h \in V_{\mathbf{u}}^h$ and $\forall q^h \in V_p^h$:

$$\int_\Omega \mathbf{w}^h \cdot \left(\frac{\partial \mathbf{u}^h}{\partial t} + \mathbf{u}^h \cdot \nabla \mathbf{u}^h - \rho \mathbf{g} \right) \mathrm{d}\Omega + \int_\Omega \varepsilon(\mathbf{w}^h) : \sigma(p^h, \mathbf{u}^h)\, \mathrm{d}\Omega - \int_{\Gamma_h} \mathbf{w}^h \cdot \mathbf{h}\, \mathrm{d}\Gamma + \int_\Omega q^h \nabla \cdot \mathbf{u}^h\, \mathrm{d}\Omega$$
$$+ \sum_{e=1}^{n_{el}} \int_{\Omega^e} [\tau_{\mathrm{SUPG}} \rho \mathbf{u}^h \cdot \nabla \mathbf{w}^h + \tau_{\mathrm{PSPG}} \nabla q^h] \cdot \left[\left(\frac{\partial \mathbf{u}^h}{\partial t} + \mathbf{u}^h \cdot \nabla \mathbf{u}^h \right) - \nabla \cdot \sigma(p^h, \mathbf{u}^h) - \rho \mathbf{g} \right] \mathrm{d}\Omega^e$$
$$+ \sum_{e=1}^{n_{el}} \int_{\Omega^e} \tau_{\mathrm{LSIC}} \nabla \cdot \mathbf{w}^h \nabla \cdot \mathbf{u}^h\, \mathrm{d}\Omega^e = 0 \tag{8}$$

In the above equation, the first four integrals on the left-hand side represent standard terms due to the Galerkin formulation and the first sum of element-wise integrals corresponds to the SUPG/PSPG stabilization, whereas the second summation is the least-squares incompressibility constraint (LSIC) stabilization term, added to prevent oscillations in high Reynolds number flows [27]. Following Tezduyar *et al.* [39], we have evaluated the stabilization terms by the following expression:

$$\tau_{\mathrm{SUPG}} = \tau_{\mathrm{PSPG}} = \left[\left(\frac{2\|\mathbf{u}^h\|}{h_e} \right)^2 + 9 \left(\frac{4}{\sqrt{Gr} {h_e}^2} \right)^2 \right]^{-1/2} \tag{9}$$

where $\mathbf{u}^h$ is the local velocity vector and h_e is the element characteristic length. In Equation (8) the LSIC stabilization is computed as

$$\tau_{\mathrm{LSIC}} = \frac{\|\mathbf{u}^h\| h_e}{2} \tag{10}$$

As noted by Akin *et al.* [19], the stabilization parameters induce a numerical viscosity proportional to $\|\mathbf{u}^h\|$, which acts similar to the eddy viscosity introduced by the Smagorinsky turbulence model. The temporal discretization of Equation (8) gives rise to a nonlinear system of equations to be solved at each time step.

The finite element formulation of Equation (5) can be expressed as follows: find $\rho^h \in S_\rho^h$, such that, $\forall w^h \in V_\rho^h$,

$$\int_\Omega w^h \left(\frac{\partial \rho^h}{\partial t} + \mathbf{u}^h \cdot \nabla \rho^h \right) \mathrm{d}\Omega + \int_\Omega \nabla w^h \cdot \left(\frac{1}{Sc\sqrt{Gr}} \right) \nabla \rho^h\, \mathrm{d}\Omega - \int_{\Gamma_h^\rho} w^h \cdot h\, \mathrm{d}\Gamma$$
$$+ \sum_{e=1}^{n_{el}} \int_{\Omega^e} \bar{\tau}_{\mathrm{SUPG}} \mathbf{u}^h \cdot \nabla w^h \left(\frac{\partial \rho^h}{\partial t} + \mathbf{u}^h \cdot \nabla \rho^h - \nabla \cdot \left(\left(\frac{1}{Sc\sqrt{Gr}} \right) \nabla \rho^h \right) \right) \mathrm{d}\Omega^e$$
$$+ \sum_{e=1}^{n_{el}} \int_{\Omega^e} \delta(\rho^h) \nabla w^h \cdot \nabla \rho^h\, \mathrm{d}\Omega^e = 0 \tag{11}$$

DOI: 10.1002/fld

where S_ρ^h and V_ρ^h are the weight and trial finite element functions. The first two integrals represent the Galerkin formulation of Equation (5) and the first sum of element-wise integrals is due to the SUPG stabilization, whereas the second element-wise summation is the discontinuity capturing (DC) term. The diffusivities induced by both SUPG and DC terms may be also interpreted as representing the effects of the fine scales in the density fluctuation transport as in the Smagorinsky model [14–16]. Note although that DC yields a nonlinear subgrid diffusivity. In this work, we use a residual-based DC term to represent these effects, the $YZ\beta$ DC introduced in [40]. The temporal discretization of Equation (11) leads to a system of nonlinear equations to be solved at each time step due to the nonlinear diffusivity term. The stabilization parameter $\bar{\tau}_{\mathrm{SUPG}}$ is computed by a relation similar to Equation (9), where $\sqrt{Gr}$ is replaced by $Sc\sqrt{Gr}$. In the case of the $YZ\beta$ DC, the nonlinear diffusivity δ is evaluated as

$$\delta(\rho^h)=\left(\frac{h_e}{2}\right)^{\beta}|\bar{\rho}^{-1}R^e(\rho^h)|\left(\sum_{j=1}^{3}\left|\bar{\rho}^{-1}\frac{\partial\rho^h}{\partial x_i}\right|^2\right)^{\beta/2-1} \tag{12}$$

where $R^e(\rho^h)$ is the element residual of Equation (11), that is,

$$R^e(\rho^h)=\frac{\partial\rho^h}{\partial t}+\mathbf{u}^h\cdot\nabla\rho^h-\nabla\cdot\left(\frac{1}{Sc\sqrt{Gr}}\right)\nabla\rho^h \tag{13}$$

Note that if $\beta=1$ and the reference density $\bar{\rho}=1$, the $YZ\beta$ DC term renders to the consistent approximated upwind method [41]. Also, in the numerical examples presented in the following section, we will investigate the effects of omitting the time-derivative term from the definition of the element residual in (13).

3. SOLUTION PROCEDURE

The solution of all test problems presented in this work employed the EdgeCFD software. It is a Fortran90 finite element code consisting of an outer time integration loop of two staggered-coupled systems of equations. In this software, most of the computational cost comes from the **u**–p coupled solution of the incompressible flow equations, whereas the cheaper part is due to the transport of the density fluctuation, ρ. Time integration is a predictor–multicorrector algorithm with adaptive timestepping by a proportional–integral–Derivative (PID) controller (further details available in [42]). Within the flow solution loop, the multi-correction steps correspond to the inexact-Newton method as described in [43]. In this method, the tolerance of the linear solver is adapted according to the history of the solution residua. As linear solver, EdgeCFD employs the generalized minimal residual (GMRES) method since both equation systems, stemming from the incompressible flow and density fluctuation transport, are non-symmetric. Furthermore, a nodal block-diagonal and diagonal preconditioners are used, respectively, for flow and transport. Most of the computational effort spent in the solution phase is devoted to matrix–vector products. In order to compute such operations more efficiently, we have used an edge-based data structure as detailed in [43]. According to Ribeiro and Coutinho [36], this data structure, when applied to problems as those described in this work, is able to reduce indirect memory access, memory requirements to hold the coefficients of the stiffness matrices and the number of floating point operations when compared with other traditional data structures such as element by element or compressed sparse row. The computations are performed in parallel using a distributed memory

DOI: 10.1002/fld

paradigm through the message passing interface library. The parallel partitions are generated by the Metis library [44], whereas the information regarding the edges of the computational grid is obtained from the EdgePack library as described in [45]. EdgePack also reorders nodes, edges and elements to improve data locality, exploiting efficiently the memory hierarchy of current processors.

4. TEST PROBLEMS

This section presents the problems employed to validate the finite element solution scheme proposed in this work for the solution of gravity current flows. The computations were performed in message passing parallelism using eight cores of Itanium-2 Montecito CPUs (1.6 GHz/8 MB) in an SGI Altix 450 system.

4.1. Planar lock exchange

One of the first measurements related to gravity currents was done in channels close to the coastal line where the mixture between fresh and sea water when a gate opens and the fluids start to flow due to the gravity takes place [1]. Such flows are named as lock-exchange flows and have been widely used to validate numerical simulations since they are very simple to reproduce in the laboratory. Therefore, there is a reasonable number of experimental data available for the main structures developed in this flow, such as form factor, dimension and frequency of lobes and clefts structures, as well as the position and displacement of the mixture head [5, 4]. In [7, 8] Härtel *et al.* discuss in detail the formation of these structures for configurations including slip and no-slip boundary conditions at the bottom and the top of the domain. In the same work, the authors present results obtained by DNS using a pseudo-spectral code. Other works reporting results for the same problem using DNS include [10, 12]. These works employ structured grids where it is common to apply a small perturbation at the beginning of the simulation in order to force a non-symmetric and more realistic flow. Such perturbation is not necessary in our tests since the non-uniform element orientation in an unstructured grid discretization is able to produce this effect.

Figure 1 presents the problem domain, with the dimensions $L_x = 30.0$, $L_y = 3.0$ and $h = 2.0$. This domain was discretized with an unstructured grid composed by 2 630 883 tetrahedra, 3 202 772 edges and 471 585 nodes. The difference in the specific mass between the heavy and the light fluid was not beyond 5% in order to follow the Boussinesq hypothesis. At the bottom and top faces, no-slip boundary conditions were applied, whereas in the other faces a slip condition was assumed. Initially the domain was half filled with the denser fluid. We set for the flow solver an

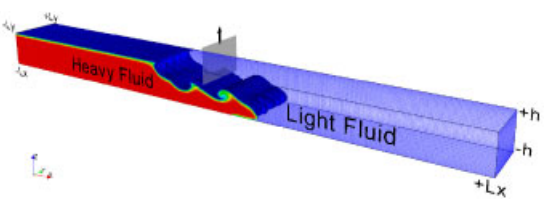

Figure 1. Planar lock exchange—problem description.

DOI: 10.1002/fld

inexact-Newton initial linear tolerance of 0.1, considering as stopping criteria a maximum of 7 inexact-Newton iterations per time step or a 3 orders of magnitude decrease on the relative residual and relative solution increment. The number of Krylov-space vectors for the inner nodal-block preconditioned GMRES method was set to 35. For the density fluctuation transport, we allowed a maximum of 10 nonlinear iterations or also a 3 orders of magnitude decrease on the relative residual and relative solution increment. The linearized systems were solved for a fixed tolerance of 10^{-4} with a diagonal preconditioned GMRES with 35 Krylov-space vectors. All computations were carried out until 20 time units and the Courant–Friedrichs–Lewy condition was chosen adaptively by the PID control algorithm in the range 0.5–2.

We performed a series of experiments investigating the influence on the front development of the LSIC term on the flow formulation and the full or just the advective residual in the nonlinear subgrid diffusivity for the density fluctuation transport. In these experiments, we set $Gr = 1.5 \times 10^6$ and $Sc = 0.71$ following [7, 8, 10, 12]. Figure 2 shows the results for three different representative

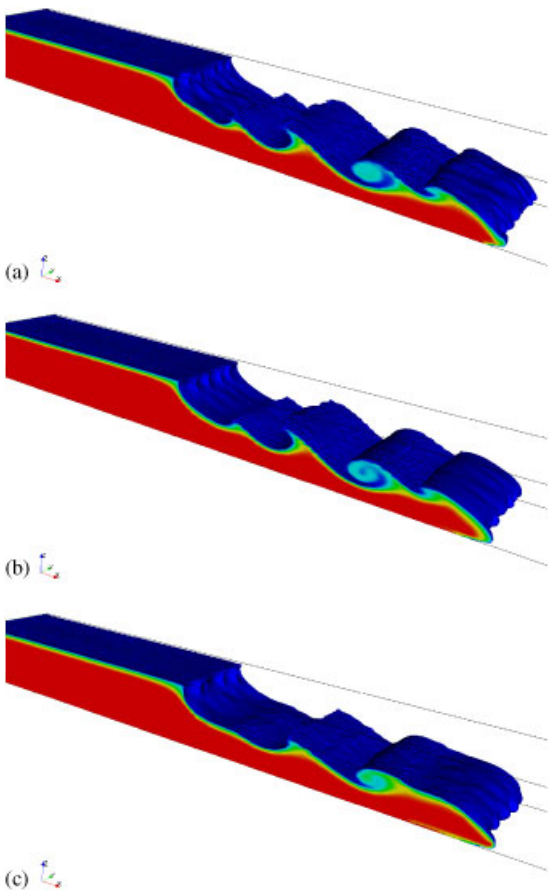

Figure 2. Influence of formulation terms in the front evolution, density isosurface $\rho = 0.5$: (a) solution at $t = 10.113$, SUPG/PSPG, $YZ\beta$ with full residual; (b) solution at $t = 10.109$, SUPG/PSPG, $YZ\beta$ with advective residual; and (c) solution at $t = 10.221$, SUPG/PSPG, LSIC and $YZ\beta$ with full residual.

DOI: 10.1002/fld

simulations at around 10 time units. In Figure 2(a) and (b), we did not consider the LSIC term in the flow formulation and the nonlinear subgrid diffusivity for the density fluctuation transport is computed with the full residual (Figure 2(a)) or the advective part (Figure 2(b)). In Figure 2(c), we show the solution computed considering LSIC and the full residual for the subgrid diffusivity.

Comparing the three solutions in Figure 2, we clearly see that when the effects of LSIC term were considered, too much dissipation is present. The solutions without LSIC present well-defined Kelvin–Helmholtz billows and the formation of typical lobes and clefts. Also, the solution with the nonlinear subgrid diffusivity for the density fluctuation computed with the full residual presents a slightly sharper definition of lobes and clefts when compared with the one computed with the advective residual. These several formulation variants also have different computational performances, since they affect the nonlinearities. Table I presents computational data for the three cases in Figure 2(a)–(c), labeled, respectively, as Run (a), (b) and (c). We may observe that the solution with LSIC was not only more dissipative but also slower, since the LSIC term added more nonlinearity to the flow formulation. The other solutions achieved comparable performances. However, Run (a) required on average slightly less effort to solve the nonlinear problems than Run (b). Also, it is interesting to note that the more dissipative solution reached the desired simulation time with larger time steps.

Figure 3 presents the results obtained in this work for Run (a) qualitatively compared with other numerical results presented by Härtel *et al.* [7] (Figure 3(b)) and Cantero [10] (Figure 3(c)) for the time units 0, 5, 10, 15 and 20. Flow is visualized by a density isosurface $\rho = 0.5$. For comparison purposes, it is important to note that Figure 3(b) presents the front position for a shorter domain ($L_x \in [-15, 15]$) than those shown in the other figures ($L_x \in [-20, 20]$)]). We can note a good qualitative agreement between our results and the others. It is important to emphasize that Härtel *et al.* [7] used a computational grid with 4.25 million points and Cantero *et al.* [10] a grid with 1.7 million points. Thus, in the present LES approach, we have reached fairly good representation of the global front behavior using a grid resolution much smaller than those presented in these references.

Figure 4 presents the evolution of the mixture front position with time. We have determined the head position by inspection of the nodes formed by the evolution in time of the density isosurfaces corresponding to $\rho = 0.5$. This is a crude method for determining the front evolution compared with the more sophisticated methods in Cantero *et al.* [12] and Ooi [14], based, respectively, on spanwise averages of current height and front position. Nevertheless, we may note that after an initial acceleration period, the front starts to displace at a near constant velocity, in agreement with the DNS results of Cantero *et al.* [12] and the highly detailed LES results of Ooi [14], also shown in Figure 4. This behavior is characteristic of the slumping phase of the flow, as discussed in [7, 8, 12, 14]. Note although that Ooi's results are for a Grashof number $Gr = 1.25 \times 10^6$. In

Table I. Computational performance comparisons in the planar lock-exchange problem.

	Run (a)	Run (b)	Run (c)
Wall time (h)	14.14	14.74	20.63
Time steps	1601	1600	1458
Inexact-Newton iterations in flow solver	3–7	3–5	7
Nonlinear iterations in density solver	3–7	2–3	5–7

DOI: 10.1002/fld

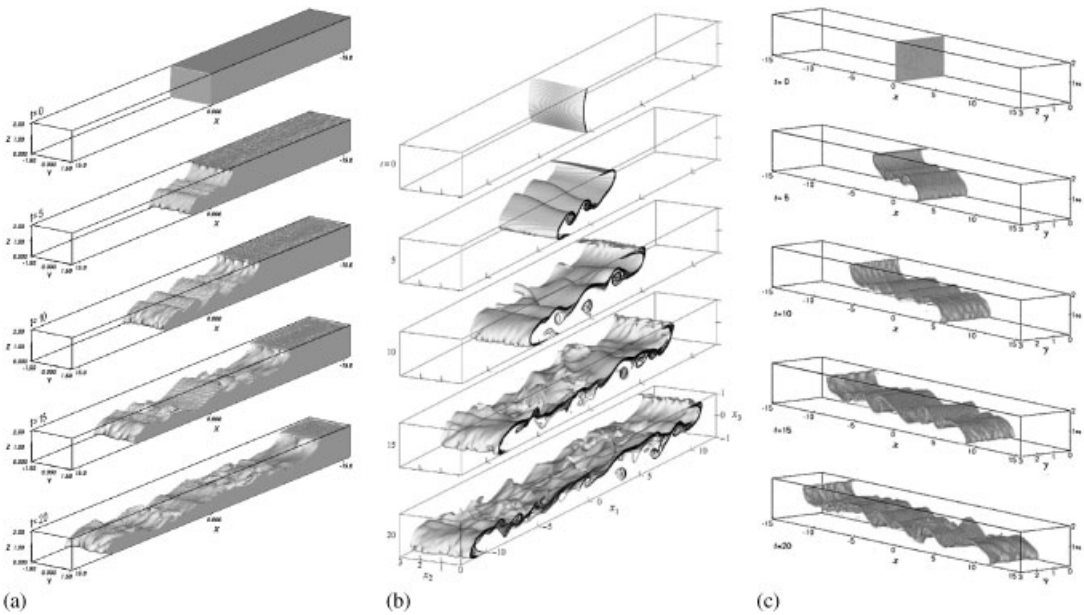

Figure 3. Qualitative comparison of density isosurfaces $\rho = 0.5$ for times 0, 5, 10, 15 and 20 between present results (a) with those shown in Härtel *et al.* [7] (b) and Cantero *et al.* [10] (c).

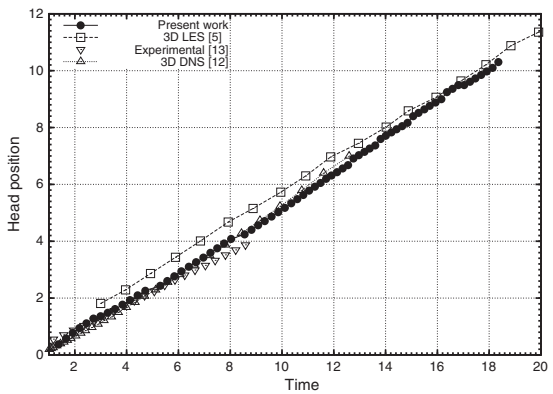

Figure 4. Head position evolution in the planar problem for $Gr = 1.5 \times 10^6$ and $Sc = 0.71$.

Figure 4, we also include the experimental results of Shin *et al.* [4]. It is worth noting the good agreement between the present results at early times and the experimental data. We may compute the Froude number, defined as $Fr = u_f / U_0$ using the near constant slope of our solution in Figure 4, that is, the velocity of the mixture front, u_f. We have found $Fr = 0.579$, which is in excellent agreement with those found in Hartel *et al.* [7], $Fr = 0.57$, Cantero *et al.* [12], $Fr = 0.576$, and Ooi [14], $Fr = 0.58$.

DOI: 10.1002/fld

4.2. *Cylindrical lock exchange*

According to Cantero *et al.* [12], the main character of the planar case described in the previous section is that the planform area increases linearly. However, in the case of a discharge of dense fluid in a cylindrical configuration, the planform area increases quadratically. This difference completely changes the dynamics of the developed flow when compared with the planar case. Moreover, for the cylindrical case, the mixture intensity tends to diminish according to the front evolution, whereas at the initial stages there exists an abrupt concentration of inertia and vorticity in regions close to the flow head with the formation of a big bulb that pushes the fluid forward and promotes an increase in the contact between the fluid phases. Consequently, more mixing and dissolution effects take part as described in [10, 12, 37, 46]. In this case, the flow dynamics is much similar to when a cloud of heavy gas is discharged in the atmosphere. It also mimics the point source river discharge in a lake or an open sea, where particulate density flows can spread radially and form important turbidity flows.

The problem considered here consists of a cylindrical column of dense fluid centralized in a circular domain. Since this flow tends to develop quasi-axisymmetrically, we have used, following [12, 37], a model corresponding to a 90° sector as illustrated in Figure 5. The domain dimensions are $L_x = 20.0$, $L_y = 20.0$ and $h = 2.0$. The initial radius of the heavier fluid is $r_0 = 2.0$ and the unstructured grid was built with 2 125 139 tetrahedra, 2 607 939 edges and 390 527 nodes. Following the planar case and References [10, 12, 46], the Grashof and Schimdt numbers are $Gr = 1.5 \times 10^6$ and $Sc = 0.71$. We employed in this simulation the SUPG/PSPG formulation for the flow and the SUPG formulation with $YZ\beta$ with full residual for the density fluctuation. In this run, we adopted a fixed time step of 0.01 and all other computational parameters were the same from the planar case. Wall clock time for this run was 10.16 h to reach 20 time units.

Figure 6 shows a qualitative comparison of the density fluctuation displacement between the results obtained in this work with those presented by Cantero *et al.* in [10, 12, 37] using a pseudo-spectral method with a computational grid 60 times finer. We can observe by the evolution of the density fluctuation isosurface $\rho = 0.15$ that, although with less spatial resolution, the main three-dimensional features of the flow are well represented, e.g. lobes and clefts and Kelvin–Helmholtz billows. It is known from experimental and numerical results (see [1, 10, 12, 37, 46]) that in this problem, the mixture front advance presents three phases with distinct behavior for the velocity and displacement. In a short initial phase, the flow head accelerates, then in the slumping phase

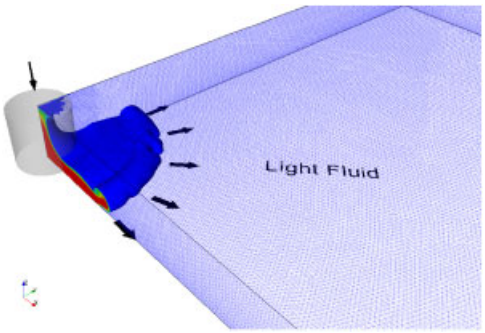

Figure 5. Cylindrical lock exchange—problem description.

DOI: 10.1002/fld

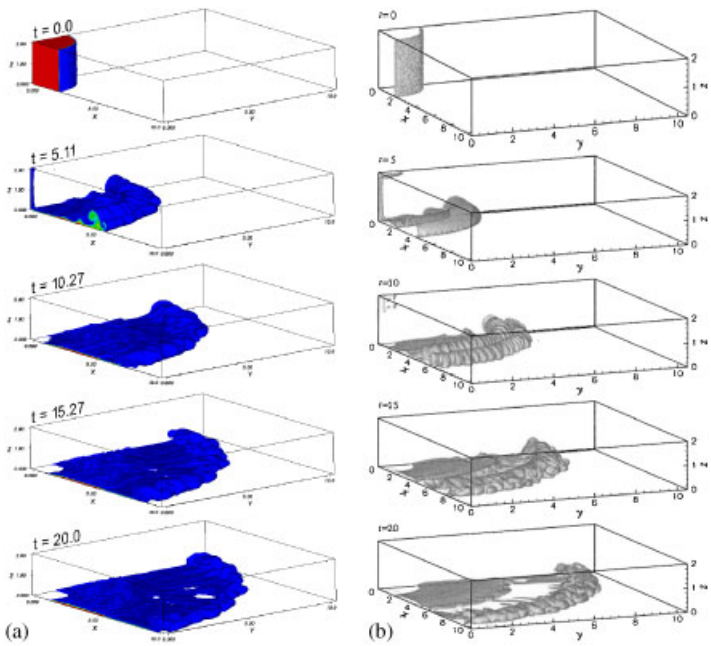

Figure 6. Qualitative comparison of density isosurfaces $\rho = 0.15$ for time units 0, 5, 10, 15 and 20 between the present results (a) and Cantero *et al.* [10, 12] (b).

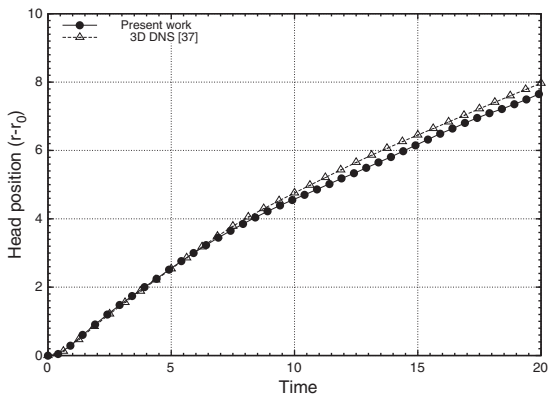

Figure 7. Radial head position evolution in the cylindrical problem for $Gr = 1.5 \times 10^6$ and $Sc = 0.71$.

the front velocity varies very slowly and in a later inertial/viscous phase the dense fluid starts to decelerate. Such behavior was also verified in our tests as can be seen in Figure 7, where the flow head mean radial position is plotted against time. The radial position is measured by inspection of the front node evolution corresponding to the density isosurface $\rho = 0.15$ projections along the two horizontal axis, X and Y. In Figure 7 we plot the mean of these values together with the head

DOI: 10.1002/fld

Table II. Current head height comparison in the cylindrical lock-exchange problem.

Time	Cantero *et al.* [37]	Present work
5.50	0.40	0.43
7.5	0.26	0.26
10.0	0.33	0.32
15.0	0.35	0.37
20.0	0.32	0.37

position obtained by spanwise current height averages from the DNS results of Cantero *et al.* [12]. We may observe fairly good agreement between the present results and those in [12].

Another quantitative comparison is given in Table II, which shows the current head height at different times for the present work together with the DNS results of Cantero *et al.* [37]. We note excellent agreement between both solutions. We are able to capture the decrease of the current head height in the transition from the slumping to the inertial flow phase and its subsequent increase at later times. Another feature worth noting is that the number of lobes in the present simulation is approximately constant. We counted, by inspection, 16–18 lobes, which is a little less than the number of lobes observed by Cantero *et al.* [37].

5. CONCLUSIONS

This work presented an application of stabilized edge-based finite elements in the modeling of phenomena related to gravity currents. This is a first step in a research intending to simulate particulate gravity currents, which are able to transport large amounts of sand to the deep ocean, flowing over very irregular sea floors with associated deposition and erosion processes. In this practical problem, multiple analyses are necessary to understand how large amounts of sand can accumulate far from inland.

The turbulent nature of such currents poses a challenge for a practical application of such simulations. With this in mind, the choice of a simple LES approach with no explicit subgrid model other than the one induced by the stabilized method itself has shown its ability to reproduce the main aspects of the current structure, such as the formation of lobes, clefts and Kelvin–Helmoltz billows, as well as the head position evolution for planar and cylindrical lock-exchange configurations. We investigated, for the planar case, several stabilized formulation variants. We have found that solutions with the LSIC stabilization term were over-dissipative. Also, solutions with the $YZ\beta$ DC operator with full residual presented more pronounced lobes and clefts. Nevertheless, fairly good agreement was achieved for the planar and cylindrical cases, where we compared our solutions with highly resolved DNS and LES results as well as experimental data (planar case only). It is also important to emphasize that the reduced time and reasonable accuracy of the present approach is a critical issue when simulating multiple flow configurations found in practice. Certainly there is room for improvement in our approach to turbulence. The recent residual-based variational multiscale method of Bazilevs *et al.* [47] represents a more mathematically coherent approach to LES, where the effects of subscales are consistently accounted. We intend, in the near future, to extend our present simulation capabilities in this direction. Another practical aspect of interest is

DOI: 10.1002/fld

the ability of the finite element method to handle complex geometries, like the ones encountered in deep sea or ocean floors. The irregularities in the sea floor bathymetry are known to have a strong influence on current dynamics and the present approach opens new possibilities to tackle such important problems.

ACKNOWLEDGEMENTS

The authors would like to thank the Petroleum National Agency (ANP, Brazil) for its financial support and Petrobras S.A. Prof. Coutinho acknowledges the partial support from CNPq. The Center for Parallel Computations (NACAD) at Federal University of Rio de Janeiro provided the computational resources employed in this work. We are indebted to Dr M. Cantero from the University of Illinois at Urbana-Champaign, who graciously provided us with his DNS simulation data.

REFERENCES

1. Simpson J. *Gravity Currents* (2nd edn). Cambridge University Press: Cambridge, 1997.
2. Lucchesi CF. Petróleo, estudos avançados. *Technical Report*, IEA/USP, 1998.
3. Neufeld J. Lobe-cleft patterns in the leading edge of a gravity current. *Master's Thesis*, University of Toronto, 2002.
4. Shin JO, Dalziel SB, Linden PF. Gravity current produced by lock exchange. *Journal of Fluid Mechanics* 2004; **521**:1–34.
5. Marino BM, Thomas LP, Linden PF. The front condition for gravity currents. *Journal of Fluid Mechanics* 2005; **536**:49–78.
6. Birman VK, Meiburg E. High-resolution simulation of gravity currents. *Journal of the Brazilian Society of Mechanical Sciences and Engineering* 2006; **28**(2):169–173.
7. Härtel C, Meiburg E, Necker F. Analysis and direct numerical simulation of the flow at a gravity-current head. Part 1: flow topology and front speed for slip and no-slip boundaries. *Journal of Fluid Mechanics* 2000; **418**:189–212.
8. Härtel C, Carlsson F, Thunblom M. Analysis and direct numerical simulation of the flow at a gravity-current head. Part 2: the lobe-and-cleft instability. *Journal of Fluid Mechanics* 2000; **418**:213–229.
9. Ozgokmen T, Fischer P, Duan J, Iliescu T. Three-dimensional turbulent bottom density currents from a high-order nonhydrostatic spectral element model. *Journal of Physical Oceanography* 2004; **34**:2006–2026.
10. Cantero MI, Balanchandar S, García MH, Ferry JP. Direct numerical simulation of planar and cylindrical density currents. *Journal of Applied Mechanics* 2006; **73**:923–930.
11. Cantero MI, García CM, García MH, Balachandar S. Characterization of flow structures at the front of cylindrical gravity current fronts. *Mecânica Computacional* 2006; **25**:2267–2291.
12. Cantero MI, Lee JR, Balanchandar S, García MH. On the front velocity of gravity currents. *Journal of Fluid Mechanics* 2007; **586**:1–39.
13. Sagaut P, Deck S, Terracol M. *Multiscale and Multiresolution Approaches in Turbulence*. Imperial College Press: London, U.K., 2006.
14. Ooi SK. High resolution numerical simulations of lock-exchange gravity-driven flows. *Ph.D. Thesis*, University of Iowa, U.S.A., 2006.
15. Ooi SK, Constantinescu G, Weber L. Analysis of the evolution of a high grashof number finite-channel lock-release current from initial stages to the inviscid phase. *The 7th International Conference on Hydroscience and Engineering* (*ICHE-2006*), 10–13 September 2006, Philadelphia, U.S.A., 2006; 1–10.
16. Pierce CD, Moin P. Progress-variable approach for large-eddy simulation of non-premixed turbulent combustion. *Journal of Fluid Mechanics* 2004; **504**:73–97.
17. Pain CC, Piggott MD, Goddard AJH, Gorman GJ, Fang F, Marshall DP, Eaton MD, Power PW, de Oliveira CRE. Three-dimensional unstructured mesh ocean modeling. *Ocean Modelling* 2005; **10**:5–33.
18. Cantero MI, García MH, Buscaglia GC, Bombardelli FA, Dari EA. Multidimensional CFD simulation of a discontinuous density current. *Proceedings of the XXX IAHR Congress*, Thessaloniki, Greece, 2003.
19. Akin JE, Tezduyar TE, Ungor M, Mittal S. Stabilization parameters and smagorinsky turbulence model. *Journal of Applied Mechanics* 2003; **70**:2–9.

DOI: 10.1002/fld

20. de Sampaio PAB, Hallak PH, Coutinho ALGA, Pfeil MS. A stabilized finite element procedure for turbulent fluid–structure interaction using adaptive time–space refinement. *International Journal for Numerical Methods in Engineering* 2004; **44**:673–693.
21. Hoffman J, Johnson C. A new approach to computational turbulence modeling. *Computer Methods in Applied Mechanics and Engineering* 2006; **195**:2865–2880.
22. Tejada-Martinez AE, Jansen KE. On the interaction between dynamic model dissipation and numerical dissipation due to streamline upwind/Petrov–Galerkin stabilization. *Computer Methods in Applied Mechanics and Engineering* 2005; **194**:1225–1248.
23. Rispoli F, Corsini A, Tezduyar TE. Finite element computation of turbulent flows with the discontinuity-capturing directional dissipation (DCDD). *Computers and Fluids* 2007; **36**:121–126.
24. Guasch O, Codina R. A heuristic argument for the sole use of numerical stabilization with no physical LES modeling in the simulation of incompressible turbulent flows. 2007; under review.
25. de Sampaio PAB, Junior MAG, Lapa CMF. A CFD approach to the atmospheric dispersion of radionuclides in the vicinity of NPPS. *Nuclear Engineering and Design* 2007; DOI: 10.1016/j.nucengdes.05.009.
26. Carey GF. A perspective on adaptive modeling and meshing (AMM). *Computer Methods in Applied Mechanics and Engineering* 2006; **195**(4–6):214–235.
27. Tezduyar TE. Finite elements in fluids: stabilized formulations and moving boundaries and interfaces. *Computers and Fluids* 2007; **36**:191–206.
28. Tezduyar TE, Sathe S. Modelling of fluid–structure interactions with the space–time finite elements: solution techniques. *International Journal for Numerical Methods in Fluids* 2007; **54**:855–900.
29. Lohner R. *Applied CFD Techniques*. Wiley: New York, 2001.
30. Ribeiro FLB, Galeão AC, Landau L. Edge-based finite element method for shallow-water equations. *International Journal for Numerical Methods in Fluids* 2001; **36**:659–685.
31. Catabriga L, Coutinho ALGA. Implicit SUPG solution of euler equations using edge-based data structures. *Computer Methods in Applied Mechanics and Engineering* 2002; **32**:3477–3490.
32. Soto O, Lohner R, Cebral JR, Camelli F. A stabilized edge-based implicit incompressible flow formulation. *Computer Methods in Applied Mechanics and Engineering* 2004; **193**:2139–2154.
33. Kraft RA, Coutinho ALGA, de Sampaio PAB. Edge-based data structures for a symmetric stabilized finite element method for the incompressible Navier–Stokes equations with heat transfer. *International Journal for Numerical Methods in Fluids* 2007; **53**:1473–1494.
34. Elias RN, Martins MAD, Coutinho ALGA. Parallel edge-based solution of viscoplastic flows with the SUPG/PSPG formulation. *Computational Mechanics* 2006; **38**:365–381.
35. Elias RN, Coutinho ALGA. Stabilized edge-based finite element simulation of free-surface flows. *International Journal for Numerical Methods in Fluids* 2007; **54**:965–993.
36. Ribeiro FLB, Coutinho ALGA. Comparison between element, edge and compressed storage schemes for iterative solutions in finite element analyses. *International Journal for Numerical Methods in Engineering* 2005; **63**(4): 569–588.
37. Cantero MI, Balanchandar S, García MH. High resolution simulations of cylindrical density currents. *Journal of Fluid Mechanics* 2007; **590**:437–469.
38. Kneller BC, Bennet SJ, McCaffrey WD. Velocity structure, turbulence and fluid stresses in experimental gravity currents. *Journal of Geophysical Research* 1999; **104**:5381–5391.
39. Tezduyar TE, Mital S, Ray SE, Shi R. Incompressible flow computations with stabilized bilinear and linear equal-order-interpolation velocity–pressure elements. *Computer Methods in Applied Mechanics and Engineering* 1992; **95**:221–242.
40. Bazilevs Y, Calo VM, Tezduyar TE, Hughes TJR. $yz\beta$ discontinuity capturing for advection-dominated processes with application to arterial drug delivery. *International Journal for Numerical Methods in Fluids* 2007; **54**: 593–608.
41. Galeão AC, do Carmo EGD. A consistent approximate upwind Petrov–Galerkin method for convection-dominated problems. *Computer Methods in Applied Mechanics and Engineering* 1988; **68**(1):83–95.
42. Valli AMP, Carey GF, Coutinho ALGA. Control strategies for timestep selection in FE simulation of incompressible flows and coupled reaction–convection–diffusion processes. *International Journal for Numerical Methods in Fluids* 2005; **47**:201–231.
43. Elias RN, Martins MAD, Coutinho ALGA. *Parallel Edge-based Inexact Newton Solution of Steady Incompressible 3D Navier–Stokes Equations*. Lecture Notes in Computer Science, vol. 3648. Springer: Berlin, 2005; 1237–1245.
44. Karypis G, Kumar V. Metis 4.0: unstructured graph partitioning and sparse matrix ordering system. *Technical Report*, University of Minnesota, Minneapolis, U.S.A., 1998.

45. Coutinho ALGA, Martins MAD, Sydenstricker RM, Elias RN. Performance comparison of data-reordering algorithms for sparse matrix–vector multiplication in edge-based unstructured grid computations. *International Journal for Numerical Methods in Engineering* 2006; **66**:431–460.
46. Patterson M, Simpson J, Dalziel S, van Heijst G. Vortical motion in the head of an axisymmetric gravity current. *Physics of Fluids* 2006; **18**:046601
47. Bazilevs Y, Calo VM, Cottrell JA, Hughes TJR, Reali A, Scovazzi G. Variational multiscale residual-based turbulence modeling for large eddy simulation of incompressible flows. *Computer Methods in Applied Mechanics and Engineering* 2007; **197**:173–201.

DOI: 10.1002/fld